Forecasting Time Series Albedo Using NARnet Based on EEMD Decomposition

Guodong Zhang, Hongmin Zhou, *Member, IEEE*, Changjing Wang, Huazhu Xue, Jindi Wang, and Huawei Wan

***Abstract*— Land surface albedo analysis and prediction are of great significance for global energy budget research and global change forecasting. Research has been performed on time series albedo analysis but seldom attempt was performed on land surface albedo prediction. This article develops an effective method for land surface albedo prediction from Moderate-Resolution Imaging Spectroradiometer (MODIS) time series albedo data (MCD43A3). It consists of time series data decomposing and time series data forecasting. The ensemble empirical mode decomposition (EEMD) method decomposes the MODIS historical time series albedo data into several intrinsic mode functions (IMFs) and one residual series, then the nonlinear autoregressive neural network (NARnet) method is used to forecast each IMF component and residue. The predictions of all IMFs and residue are summed to obtain a final forecast for the albedo series. The proposed method was performed on monthly and daily albedo prediction both in snow-free and snowy areas. The results showed that the forecast albedo consists of the MODIS albedo data well, with R^2 greater than 0.89 and RMSE less than 0.052 for snow-free areas. For snowy areas, the forecasting also performed well during snow cover periods, with R^2 greater than 0.76 and RMSE less than 0.076. For irregular change periods of snow falling and melting, it is hard to get very high prediction accuracy due to the irregular land surface change. For this problem, more land surface information should be introduced, or adjusting the model over time is necessary.**

***Index Terms*— Albedo, ensemble empirical mode decomposition (EEMD), nonlinear autoregressive neural network (NARnet), time series.**

Manuscript received September 10, 2019; revised October 25, 2019; accepted November 24, 2019. Date of publication January 10, 2020; date of current version April 22, 2020. This work was supported in part by the Key Research and Development Program of China under Grant 2016YFB0501502, in part by the National Natural Science Foundation of China under Grant 41801242, in part by the Chinese 973 Program under Grant 2013CB733403, and in part by the Key Scientific and Technological Project of Henan Province under Grant 172102110268. *(Corresponding author: Hongmin Zhou.)*

Guodong Zhang and Changjing Wang are with the State Key Laboratory of Remote Sensing Science, Beijing Engineering Research Center for Global Land Remote Sensing Products, Faculty of Geographical Science, Beijing Normal University, Beijing 100875, China, and also with the School of Surveying and Land Information Engineering, Henan Polytechnic University, Jiaozuo 454000, China (e-mail: 201704020045@home.hpu.edu.cn; 201704020046@home.hpu.edu.cn).

Hongmin Zhou and Jindi Wang are with the State Key Laboratory of Remote Sensing Science, Beijing Engineering Research Center for Global Land Remote Sensing Products, Faculty of Geographical Science, Beijing Normal University, Beijing 100875, China (e-mail: zhouhm@bnu.edu.cn; wangjd@bnu.edu.cn).

Huazhu Xue is with the School of Surveying and Land Information Engineering, Henan Polytechnic University, Jiaozuo 454000, China (e-mail: xhz@hpu.edu.cn).

Huawei Wan is with the Satellite Environment Center, Ministry of Environmental Protection, Beijing 100094, China (e-mail: wanhw@secmep.cn).

Color versions of one or more of the figures in this article are available online at http://ieeexplore.ieee.org.

Digital Object Identifier 10.1109/TGRS.2019.2958048

I. Introduction

LAND surface albedo, the ratio of reflected solar radiation to the total incident solar radiation, has been identified by the global terrestrial observing system (GTOS) as a crucial climate variable that adjusts Earth's radiative budget [1]–[4]. The radiation absorbed by the land surface is the initial energy input in the ecosystem cycle, and it is stored in the soil–vegetation biophysical system until further conversion [5]–[8]. Studies have shown that albedo may have a significant influence in regulating the energy cycle [9]. Global climate studies can obtain albedo data sets from Advanced Very High-Resolution Radiometer (AVHRR) [10]–[12], Moderate-Resolution Imaging Spectroradiometer (MODIS) [13], Global Land Surface Satellite (GLASS) 14, and other coarse-resolution sensors. Time series albedo data provide information on land surface energy and support the analysis of global and regional change. Modeling albedo time series and forecasting short-term albedo values in the future are of great significance to meteorological prediction, agricultural monitoring, urban environmental assessment, and forest management [15]. The update of land surface albedo by substituting the albedo derived from soil and vegetation type map with remotely sensed albedo product, which has essential spatial and seasonal variability, can effectively explain the regional scale tropical deforestation [16]. It is also confirmed that the use of near-real-time forecast albedo has an impact on surface carbon and energy fluxes in the global model [17]. The introduction of land surface variables, including albedo, in the prognostic model is a possible way to reduce the global model noise. Therefore, efficient techniques and methods for albedo forecasting are needed. Temporal and spatial complete albedo is needed when it is used in the global model. But due to cloud contamination, remote sensing albedo products remain a large number of absent values. Forecasting short-term albedo values in the near future is also an efficient way to fill the data absence as it always includes historical data processing.

There are many models for time series forecasting, such as statistical methods, simulation methods, and neural network methods. Some frequently used statistical methods that can characterize nonstationary time series data and predict future values have been widely used in the prediction of remote sensing parameters, including dynamic harmonics regression (DHR), seasonal-trend decomposition procedure based on loess (STL), and seasonal autoregressive integrated moving average (SARIMA). Jiang *et al.* [18] used MODIS historical

leaf area index (LAI) data as input data to predict the future values of LAI based on the DHR model. The model can decompose the LAI time series of each pixel into several components: trend, intra-annual variations, seasonal cycle, and stochastic stationary or irregular parts, finally generate accurate prediction LAI time series and produce the smoothest curve. Cristina *et al.* [19] identified the temporal variability of the dynamic features in the MEdium Resolution Imaging Spectrometer (MERIS) products for water leaving reflectance and Algal Pigment Index 1 (API 1) using the STL modeling method. Zhou *et al.* [20] used a data-based mechanism (DBM) method to model MODIS time series and predict the next moment LAI value that are used to construct the dynamic model. Wang *et al.* [21] combined the autoregressive integrated moving average (ARIMA) method with the ensemble empirical mode decomposition (EEMD) method to forecast the annual runoff time series. EEMD decomposes the original annual runoff time series for a deep insight into the data characteristics, and different ARIMA models are used to forecast each component. Through the three different reservoirs in China, the EEMD-ARIMA method can predict the annual runoff well. Although the statistical methods described above have advantages when used in modeling remotely sensed data, they also have obvious shortcomings, which include the uncertainty and divergence of prediction results due to the mutation and quantitative restriction of learning data.

Data assimilation involves field and remote sensing observations into the physical models through iterative minimization of a cost function, and it is an efficient way of estimating and forecasting land surface parameters from remotely sensed data. Xu *et al.* [22] proposed a case study of assimilating the Soil Moisture and Ocean Salinity (SMOS) soil moisture data into a coupled land-surface and hydrological model MESH with an ensemble Kalman filter (EnKF) method. The assimilation of SMOS retrievals greatly enhances the ability of the MESH model in simulating soil moisture. Xiao *et al.* [23] proposed a new algorithm to estimate LAI from time-series MODIS reflectance data. This method coupled a radiative-transfer model with a double-logistic LAI temporal-profile model to generate a temporally continuous LAI product based on the shuffled complex evolution optimization method. The accuracy of this method is significantly higher than the MODIS LAI product. Ines *et al.* [24] developed a data assimilation-crop modeling framework to improve the prediction of crop yields. This framework incorporates remotely sensed soil moisture and LAI into the decision support system for agro-technology transfer—cropping system model (DSSAT-CSM)-maize model and uses the EnKF method to simulate and predict crop yields. Though the simulation method can effectively update the analysis with new observation data induced, there are also unavoidable defects in the disposal of sample and mode errors.

The prevailing machine learning (ML) methods, which automatically learn the mechanism from the data itself, are robust in time series prediction. Sauter *et al.* [25] developed a nonparametric approach to forecast the development of snow cover and snow duration in the future. The method combined nonlinear autoregressive networks with exogenous inputs (NARX) with remote sensing and geographical information system (GIS), effectively improved the spatial resolution of snow patterns by incorporating complex structures of the underlying terrain. Zhang *et al.* [26] established a nonlinear autoregressive neural network (NARnet) model for forecasting the number of electric vehicles (EVs) in Shenzhen City. The results showed that the NARnet model for forecasting the charging demand of EVs tends to deliver good performance in future practical applications. In fact, the NARnet can be used to predict many kinds of nonlinear time series data because of its strong self-learning and multistep prediction ability when there is no available exogenous data. However, similar to other neural networks, NARnet does not have the ability to explain its reasoning process and reasoning basis, as it turns all of its reasoning into numerical computation; therefore, the predicted results are bound to lose information when the amount of learning data is limited or the time series is irregular. Time series need to be presented in more detail to discover their internal trends and seasonality.

Although those methods described above have been widely used in the prediction of many surface parameters, there is no practical method for predicting time series surface albedo. To overcome the difficulty in albedo prediction, this article explores a new noise-assisted data analysis (NADA) and prediction method: EEMD-NARnet. The EEMD method has been proven to be a quite reliable method for discovering the trends and periodic characteristics from nonlinear and nonstationary data and it has been used in many disciplines, such as seismology, economics, and hydrology [21], [27]–[29]. In this article, the EEMD model evolved from the empirical mode decomposition (EMD) is used for decomposing time series and extracting nonlinear trends, seasonal, or other useful information to supply more abundant and regular data for NARnet model. Abnormal data hidden in the time series will be represented as residue. This method greatly improves the fault tolerance of learning data compared with traditional statistical methods. The NARnet method uses only the historic state of the system for forecasting future values, and it has the characteristics of memory and feedback when there is no exogenous data, it can avoid multiparameter sample processing and mode error in the simulation method. Combining these two methods can effectively improve the recognition ability of uneven information in time series and model prediction ability [30].

II. Experimental Area and Data

A. Study Area

We chose two study areas to test this algorithm: Fair Bluff and Under-Khuan. Fair Bluff is located in Columbus County, North Carolina, United States, at a latitude of 34.3112°N and longitude of 79.03239°W. The region has a subtropical climate with a growth period of 275 days and an average annual temperature of 19 °C. It is rainy in July and August and the driest months are October and November. The average annual rainfall is 117–137 cm. The main land cover types are croplands, evergreen broadleaf forests, and woody savannah,

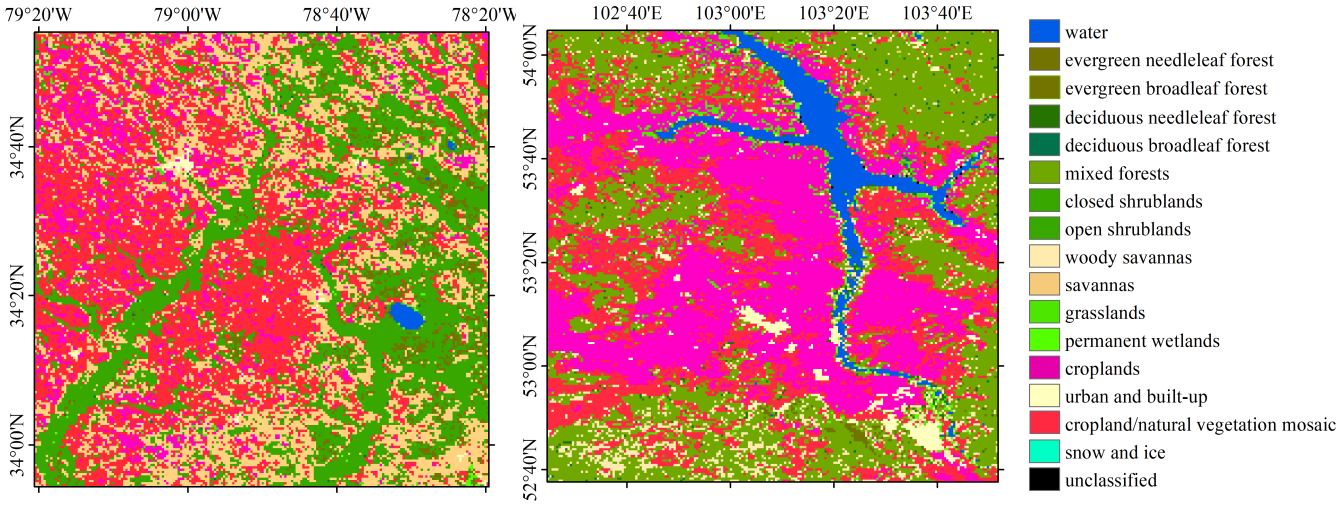

Fig. 1. Land surface cover map of (Left) Fair Bluff and (Right) Under-Khuan in 2010.

TABLE I
SELECTED PIXELS INFORMATION IN FAIR-BLUFF

number	Latitude(°)	Longitude(°)	Land cover types
pixel 1	33.990N	79.091W	Water
pixel 2	34.706N	78.349W	Evergreen Needleleaf Forests
pixel 3	33.919N	78.738W	Evergreen Broadleaf Forests
pixel 4	33.979N	78.344W	Deciduous Needleleaf Forests
pixel 5	33.924N	78.718W	Deciduous Broadleaf Forests
pixel 6	34.888N	78.713W	Mixed Forests
pixel 7	34.878N	78.768W	Closed Shrublands
pixel 8	34.914N	78.935W	Woody Savannas
pixel 9	34.606N	78.445W	Grasslands
pixel 10	34.903N	78.364W	Permanent Wetlands
pixel 11	34.878N	79.051W	Croplands
pixel 12	34.464N	78.571W	Urban and Built-up Lands

TABLE II
SELECTED PIXELS INFORMATION IN UNDER-KHUAN

number	Latitude(°)	Longitude(°)	Land cover types
pixel 1	53.324N	102.535E	Water
pixel 2	52.681N	103.605E	Evergreen Needleleaf Forests
pixel 3	52.681N	102.954E	Deciduous Needleleaf Forests
pixel 4	52.758N	102.423E	Deciduous Broadleaf Forests
pixel 5	52.681N	103.772E	Mixed Forests
pixel 6	53.128N	102.780E	Closed Shrublands
pixel 7	52.688N	103.395E	Woody Savannas
pixel 8	53.883N	103.367E	Grasslands
pixel 9	53.743N	102.738E	Permanent Wetlands
pixel 10	53.289N	103.234E	Croplands
pixel 11	53.974N	102.919E	Urban and Built-up Lands
pixel 12	53.373N	102.542E	Snow and ice

and there are also some other land cover types, such as evergreen needleleaf forests, mixed forests, and grasslands.

Under-Khuan is a town in the first administrative region of the Russian Federation, located at 53.4011°N, 103.1017°W.

This is a mountainous region with a temperate continental climate. It is cold and dry in winter and rainy in summer. The annual average temperature is below zero. In July, the average temperature ranges from 16 °C to 19 °C. In low-lying areas, even in the summer, there are frosts. The average temperature in January is from −19 °C to −20 °C. The land cover types are mainly farmland and evergreen needleleaf forest. Fig. 1 shows the land cover types of the two research areas; the research area is 100 km × 100 km (200 × 200 (500 m) pixels) for each site.

In each study area, several pixels of different land cover types are selected to evaluate the modeling and forecasting accuracy. The attributes of selected pixels in Fair Bluff are given in Table I, and the attributes of selected pixels in Under-Khuan are given in Table II.

B. MODIS Albedo/BRDF Database

The MODIS albedo (MCD43A3 Collection 6) data are used for albedo time series modeling and forecasting. The MODIS albedo product is produced with a semi-empirical bi-directional reflectance distribution function (BRDF) model [13], [31], [32]. The Ross–Li kernel model, proposed by Roujean *et al.* 35, is a linear kernel-driven model to fit and estimate BRDF [34]. It is expressed as follows:

$$R(\theta, \vartheta, \phi, \Lambda) = f_{\text{iso}}(\Lambda) + f_{\text{vol}}(\Lambda) K_{\text{vol}}(\theta, \vartheta, \phi) + f_{\text{geo}}(\Lambda) K_{\text{geo}}(\theta, \vartheta, \phi) \quad (1)$$

where $R(\theta, \vartheta, \phi, \Lambda)$ is the frontal reflectivity with a solar zenith angle θ, observed zenith angle ϑ, relative azimuth ϕ, and wavelength b and Λ. $f_{\text{iso}}(\Lambda)$ is the proportion of uniform scattering in all directions, $f_{\text{vol}}(\Lambda)$ is the proportion of volume scattering, $f_{\text{geo}}(\Lambda)$ is the proportion of geometric optical scattering, $K_{\text{geo}}(\theta, \vartheta, \phi)$ is LiSparse kernel.

The MODIS albedo (MCD43A3 Collection 6) data are estimated from all the cloud-screened, snow-flagged, and atmospherically corrected MODIS Terra and Aqua surface reflectance observed at each pixel location over a 16-day period [35]. The daily, 500-m combined albedo product provides black-sky albedo (BSA) and white-sky albedo (WSA) for the seven MODIS bands (MODIS channels 1–7) and

for three broad bands (0.3–0.7, 0.7–5.0, and 0.3–5.0 μm) 38,39,40. Blue-sky albedo can be calculated from BSA and WSA according to the proportion of sky scattered light [39]. The formula is expressed as

$$\alpha(\theta_i, \lambda) = (1 - s(\theta_i \tau(\lambda)))\alpha_{bs}(\theta_i, \lambda) + s(\theta_i \tau(\lambda))\alpha_{ws}(\theta_i, \lambda) \quad (2)$$

where $\alpha(\theta_i, \lambda)$ is the BSA of the band λ at a solar zenith angle of θ; $\alpha_{bs}(\theta_i, \lambda)$ is BSA, and $\alpha_{ws}(\theta_i, \lambda)$ is WSA. $\mathsf{s}(\theta_i, \tau(\lambda))$ is the fraction of diffuse skylight when the solar zenith angle is θ; it is a function of aerosol optical depth, and it can be calculated using a predetermined lookup table (LUT), based on a 6S atmospheric radiative transfer code.

The black-sky and white-sky shortwave albedos are derived by fusing the narrowband albedos, using the narrowband to broadband albedo conversion formula [40], [41]. Not every pixel value in MCD43A3 is available. For those situations where the retrieval failed, the *a priori* estimates come from a global database of previously collected high-quality MODIS BRDF/albedo retrievals for that pixel are used as the backup algorithm. The backup algorithm retrievals are flagged as low-quality results. If no observations are obtained during the 16-day interval, the pixel will be stored with a filled value [42].

In this article, data from 2001 to 2017 is downloaded from https://ladsweb.modaps.eosdis.nasa.gov for each site. Temporal complete albedo data are needed for time series modeling and forecasting; therefore, the filled value, which is considered as the lowest quality, is substituted using the space information [43]. The ecosystem of the Earth's surface is closely related to the type of surface, and the same type of land surface is more likely to have similar reflection and absorption characteristics [44]. Therefore, the filled pixels are replaced with the average of all values that have the same kind of land type in a window (5×5 pixels) centered on the target pixel. If there are no values available in the window, albedo values for the nearest five years will be averaged to fill the absence, and land cover map for each year is used to identify the land cover types.

The MODIS albedo product (MCD43A3 Collection 6) has a spatial resolution of 500 m and a temporal resolution of one day. Monthly albedo and daily albedo values are used in this article. The monthly albedo was obtained by taking the average of all the days in a month.

III. Methodology

The albedo forecasting algorithm consists of three steps: first, the albedo time series is decomposed based on EEMD, then the NARnet prediction method is performed on the decomposed time series to get near future forecasting for each component, finally, all forecast parts are compiled together to obtain the final forecasting.

Different methods were performed to obtain high accuracy albedo time series for snow-free and snowy areas. In snow-free areas, the time series of all monthly albedo values from 2001 to 2016 is decomposed into several intrinsic mode functions (IMFs) and one residue, then the NARnet method is used to forecast each IMF and residue. All prediction results are recombined to obtain the final forecast time series albedo. In snowy areas, we reconstructed the time series using albedos of the same month from 2001 to 2016, and the forecasting methods are the same as for the snow-free areas. A flow chart outlining the method is shown in Fig. 2.

A. EEMD

The EMD is a self-adaptive decomposition technique. It catches the intrinsic oscillatory rule according to the characteristic frequencies in the nonlinear and nonstationary data empirically and decomposes the data into several IMFs and one residue. The IMFs represent the different properties of the time series using different fast and slow oscillation components with a zero average. The components have different properties in contrast to the Fourier series, which are composed of simple sinusoidal functions [45]. The EMD decomposition process can be summarized as follows.

1) Determine all the maximum points of the original data sequence $s(t)$ and fit the upper envelope *emax(t)* of the original data with spline interpolation function.
2) Determine all the minimum points of the original data sequence $s(t)$ and fit the lower envelope *emin(t)* of the original data with a spline interpolation function.
3) Calculate the mean value $m(t)$ of the upper envelope and the lower envelope
$$m(t) = (e_{\min}(t) + e_{\max}(t))/2. \quad (3)$$
4) Obtain a new data sequence $d(t)$ from the difference of the original data sequence $s(t)$ and the average envelope $m\ (t)$
$$d(t) = s(t) - m(t). \quad (4)$$
5) The IMFs need to follow two conditions. First, in the whole time series, the number of zero-crossings and local extreme must be equal to or less than one. Second, the local mean defined by the local maxima and the envelope defined by the local minima is zero. If $d(t)$ does not meet the two conditions, then it is not an IMF, and $s(t)$ is replaced with $d(t)$ and steps 1–4 are reiterated until $d(t)$ meets the two conditions of the IMF.

Although EMD has a strong self-adaptive decomposition ability for nonlinear and non-stationary data, mode mixing is always an intractable problem in application [46]. Mode mixing occurs when jumping changes exist in the time series. In general, each IMF should have only one frequency, but sometimes one IMF component decomposed by EMD may contain different time scale features; thus, two or more frequencies may appear separately in different IMFs [47].

The mode mixing problem is not only related to the algorithm but also affected by the frequency characteristics of the original data. EEMD, a NADA method, proposed by Wu and Huang [48] is used to solve the mode mixing problem. White noise is added to the time-series data, and EMD is performed to decompose the data into IMF components. This step is repeated n times, and all the results are averaged to obtain the final decomposition. In this procedure, the time series with added white noise is distributed uniformly throughout the time–frequency space, the data at different time scales

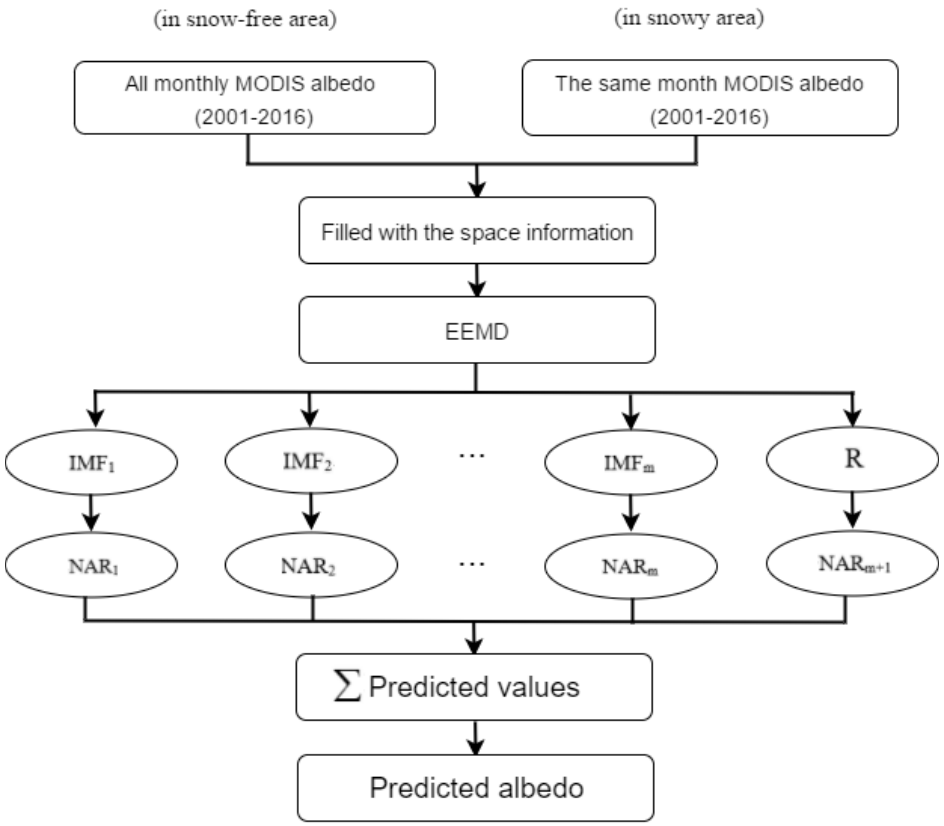

Fig. 2. Flowchart of albedo prediction using the EEMD-NARnet method.

will be automatically distributed to the appropriate reference scale, the noise signals will cancel one another, and the result of the ensemble mean can be taken as the final result. the EEMD decomposition process can be summarized as follows.

1) Add a normal distribution white noise to the original signal.
2) Decompose the new signal with an added normal distribution of white noise into several IMFs.
3) Repeat steps 1 and 2, adding different white noise sequences each time.

Take the average of each corresponding IMF component in the N decompositions as the final result.

B. NARnet

The NARnet is a suitable method for predicting future values based only on the historic state of the system, with the characteristics of memory and feedback when there is no exogenous data [49]. The NARnet model predicts future values using only past values of itself; when we take the history value as the input data, the model is constructed as follows:

$$y_n = f(y_{n-1}, \ldots, y_{n-d}) + d\varepsilon_n \tag{5}$$

where y is the output data, n is the time series, ε_n is a random variable obeying the Gauss distribution, d is a constant that represents the lag desired, and f is the neural network.

In the NARnet model, a neural network should be established for training the model, and the number of input layer, output layer, and hidden layer is needed to control the neural network training and model prediction. After completing the former step prediction, the output will be the input to adjust parameters in the next step. Because the model output is albedo only, the output layer is set to 1. The number of input layer determines how much data will be used in each layer's prediction. In this article, the input layer number of 12–24 with a step of 1 was tested, which means 12–24 months' data were used in each layer's prediction. The number of hidden layer determines the performance of the model prediction; if it is too small, the true trend of the historical data cannot be effectively displayed. If it is too big, the model is prone to over-fitting. In this article, the input layer of 12–24, and the hidden layer of 10–30 both with a step of 1 were input to NARnet model, the model trained and gave an optimal training result determined with RMSE. To guarantee the stability and accuracy of the model, we repeated the training procedure for 1000 times and found that the most frequent combination of the two parameters is 20 (input layer) and 20 (hidden layer). We then checked the statistics of RMSEs for each combination and found with the same values when referring to mean, minimum, and maximum. Thus, both the input layer and hidden layer are set to 20 in this article [26].

C. EEMD-NARnet Model for Albedo Forecasting

The EEMD-NARnet model is used for albedo forecasting. First, the EEMD is used to divide the original time series albedo into several IMFs, which have symmetrical amplitudes and are centered at a particular frequency or time scale. Meanwhile, one residue is also generated with the decomposition.

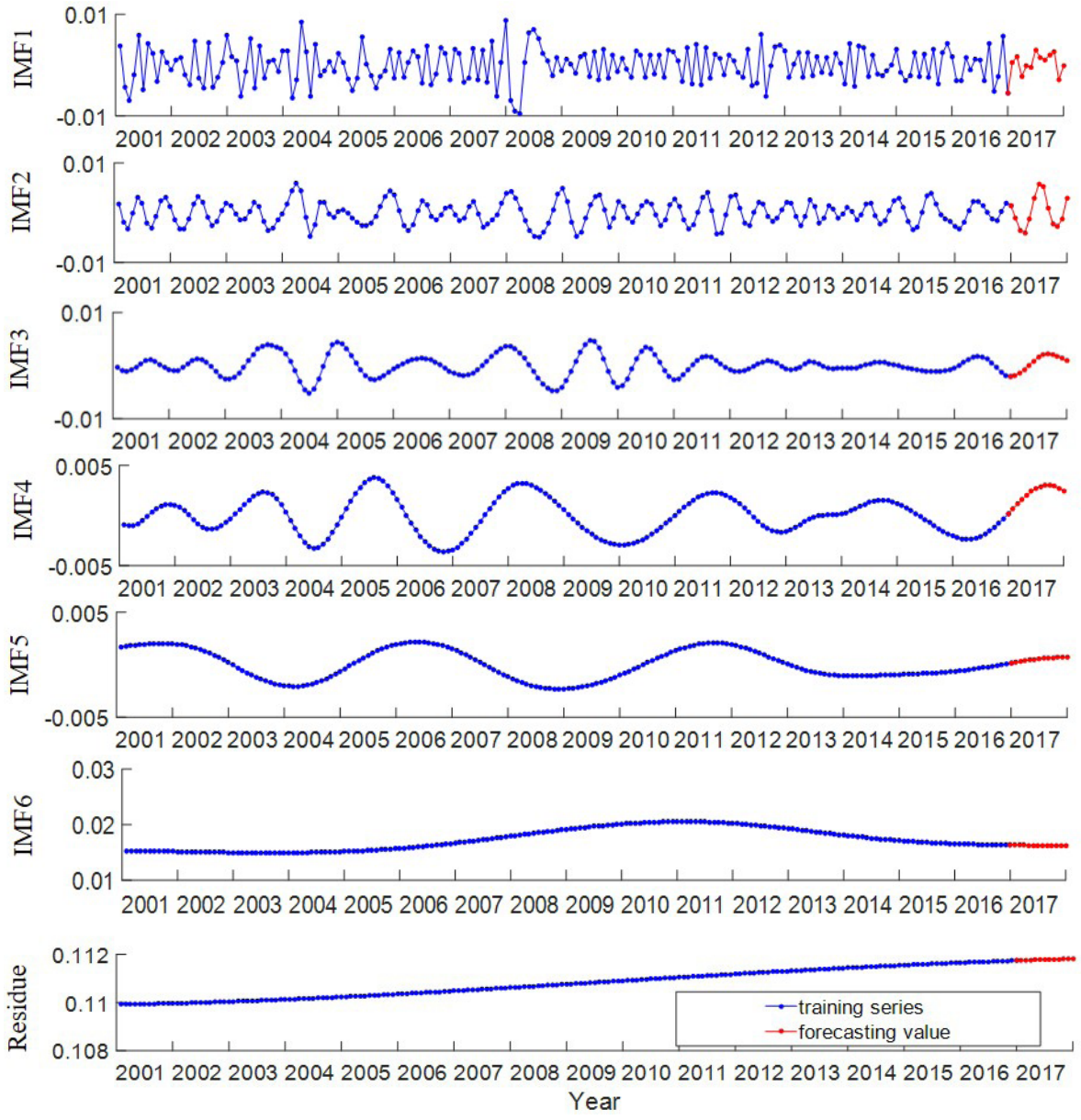

Fig. 3. Decomposition and prediction of time series albedo in a cropland pixel.

Second, for each IMF component and residue, NARnet is used to forecast the target time series. Finally, all the components and residue are summed to obtain the final prediction result.

There are two pivotal parameters that need to be set: the number of the ensemble and the intensity of the white noise. The ensemble can effectively solve the model mixing problems in EMD. The white noise distributed in the whole time frequency uniformly plays an important role in adjusting signals at different time scales. The statistical relationship among the ensemble number, n, the intensity of the white noise, c, and the standard deviation of the error, σ, can be expressed as follows:

$$\sigma = \frac{c}{\sqrt{n}}. \tag{6}$$

In this article, we implement the decomposition algorithm with an ensemble number of 100 and a white noise intensity of 0.2 times the standard deviation according to Wu and Huang [48].

Decomposition and prediction are the main features of the EEMD-NARnet when applied for albedo forecasting. The decomposition is used to simplify the forecasting task, and the ensemble is used to ensure the consistency of the neural network prediction.

IV. Result

A. Monthly Albedo Prediction at a Single Point

The albedo EEMD-NARnet forecasting model is first applied to forecast monthly albedo at a cropland pixel. Data from 2001 to 2016 is used for model training, and data of 2017 is used for validation.

The time series albedo from 2001 to 2016 is decomposed by the EEMD method first. Fig. 3 shows the decomposition and prediction results of each component. The original time

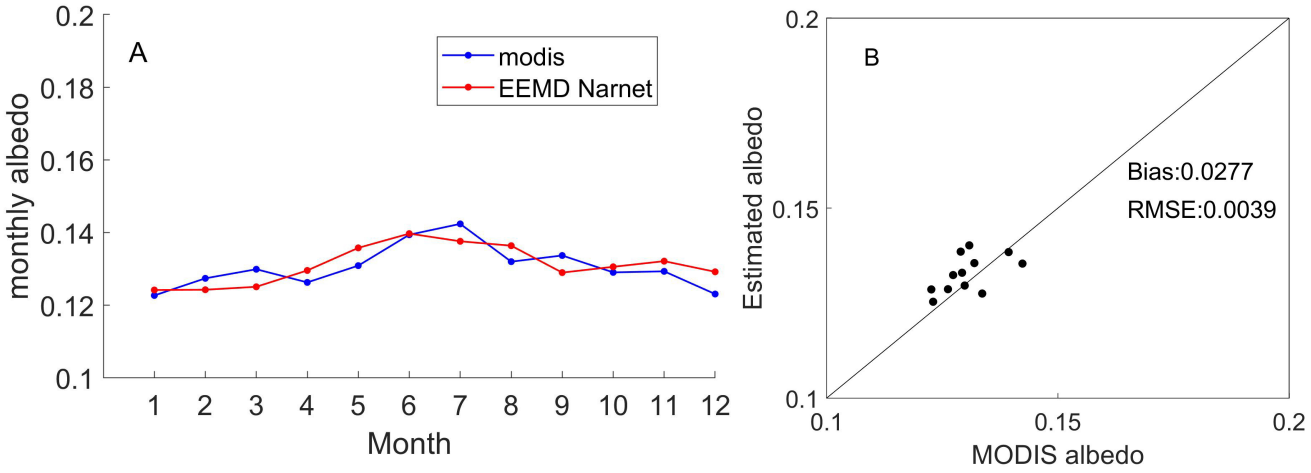

Fig. 4. Comparison of the EEMD-NARnet forecasts with MODIS time series monthly albedo in a cropland pixel. (a) Monthly albedo profile in 2017. (b) Scatter plot in 2017.

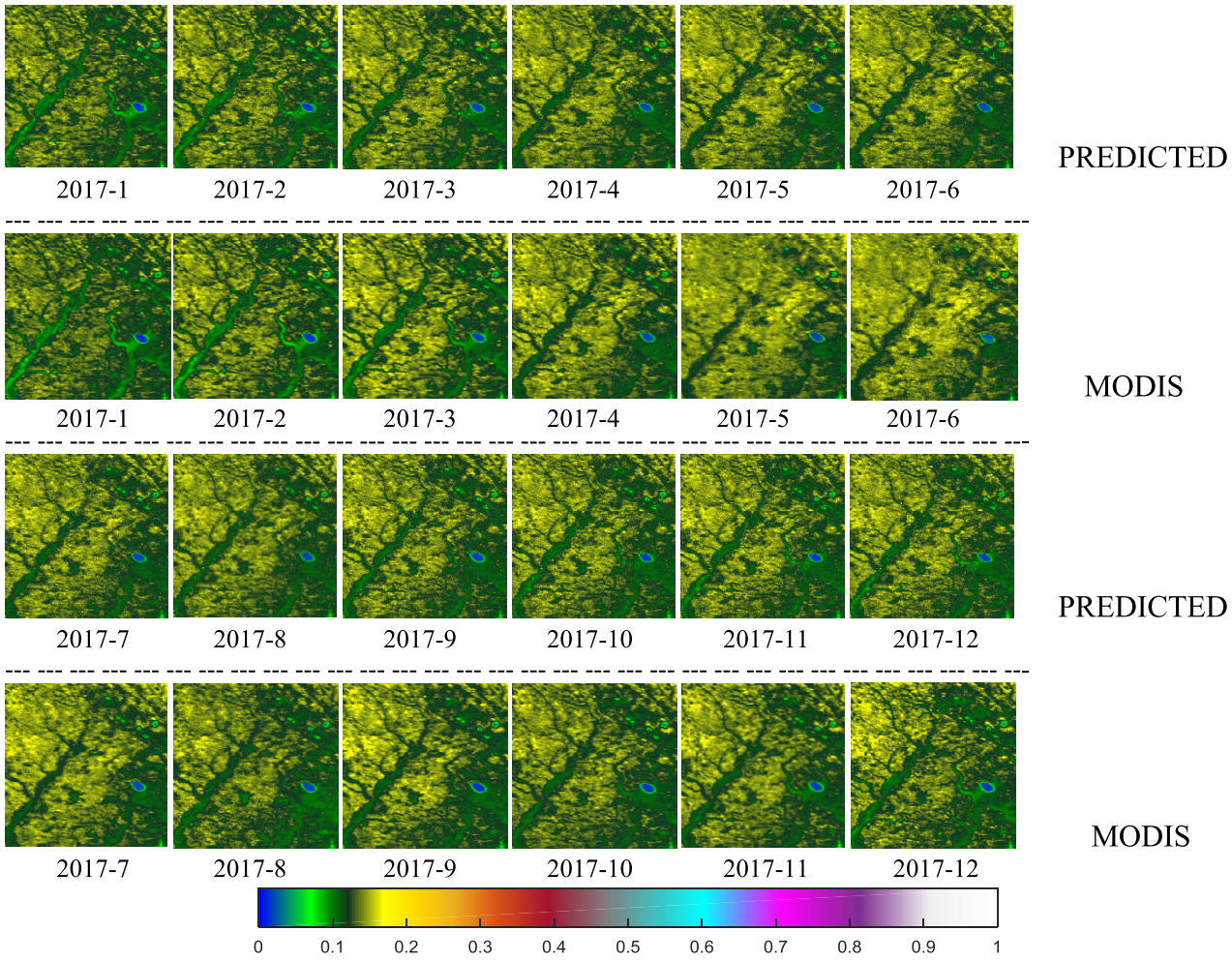

Fig. 5. Illustration of the consistency between the predicted albedo from EEMD-NARnet and the MODIS albedo in a snow-free area. The month of year is indicated for each monthly albedo map (YEAR-MONTH).

series is decomposed into five intrinsic mode components, IMF1, IMF2, IMF3, IMF4, IMF5, IMF6, and one residue. The IMFs represent the most significant and important information of the original time series, and they contain different time scales; characteristics of the series can be expressed at different resolutions. The frequencies of these components ranged from high to low, and EEMD can be regarded as a set of adaptive high-pass filters.

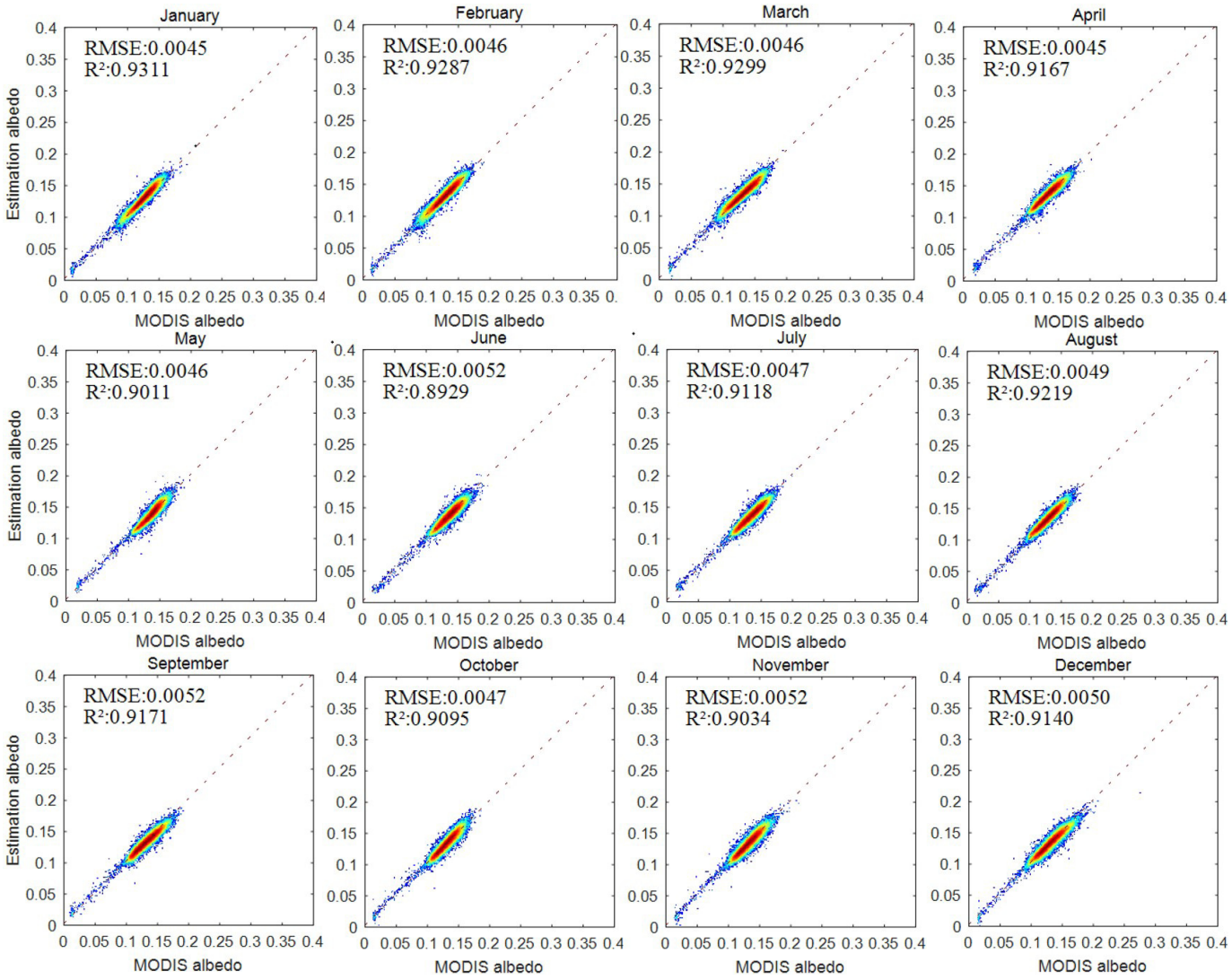

Fig. 6. Scatterplot and statistics for a snow-free area; the density plot uses color from blue to red to represent density from low to high, respectively.

IMFs and residue from EEMD are used as the input data in NARnet; after loading the accumulated data, there are three critical parameters that should be set—the number of input layer, output layer, and hidden layer. In this article, the number of input layer is set to be 20, the number of output layer is set to be 1, and the number of hidden layer is 20. The near future forecasting obtained with NARnet is shown in red in Fig. 3. The final forecasting albedo time series can be obtained by adding all the predicted components. Fig. 4 illustrates the albedo forecasting results using EEMD-NARnet models.

From Fig. 4, we can see that the prediction results are in good agreement with the MODIS data. This reflects the periodic characteristics of the monthly average albedo well. Albedo value in 2017 goes up in the first half year and then goes down in the second half year. The statistical test shows the forecast value with MODIS product. The Bias is 0.0277 and RMSE is 0.0039.

B. Monthly Albedo Prediction for a Snow-Free Area

The EEMD-NARnet method is then performed on a snow-free area in Fair Bluff. For the entire research area of 200 × 200 pixels (100 × 100 km), various land cover types such as water, evergreen needleleaf forests, evergreen broadleaf forests, deciduous needleleaf forests, deciduous broadleaf forests, mixed forests, closed shrublands, woody savannas, grasslands, permanent wetlands, and croplands are included. The predicted time series albedo is compared with MODIS albedo data in Fig. 5. From Fig. 5, we can see that the predicted albedo captured the main future of the land surface albedo variation. Albedo increases steadily from year beginning to mid-year, then decrease till the year-end. Land surface albedo has a relatively stable change pattern in the snow-free area, the variation pattern consists well with MODIS product. The study area is located in California, during the summer the climate is dry and hot and the vegetation is sparse, the land surface is dominated by bare soil, and thus, albedo value remains at a high level. During the winter, the climate becomes mild, the precipitation increases, the vegetation enters the growing season, and the land surface albedo begins to decrease [50]. The monthly average albedo prediction maps can reflect the characteristics of season and vegetation growth change. The albedo distribution for both predicted and MODIS

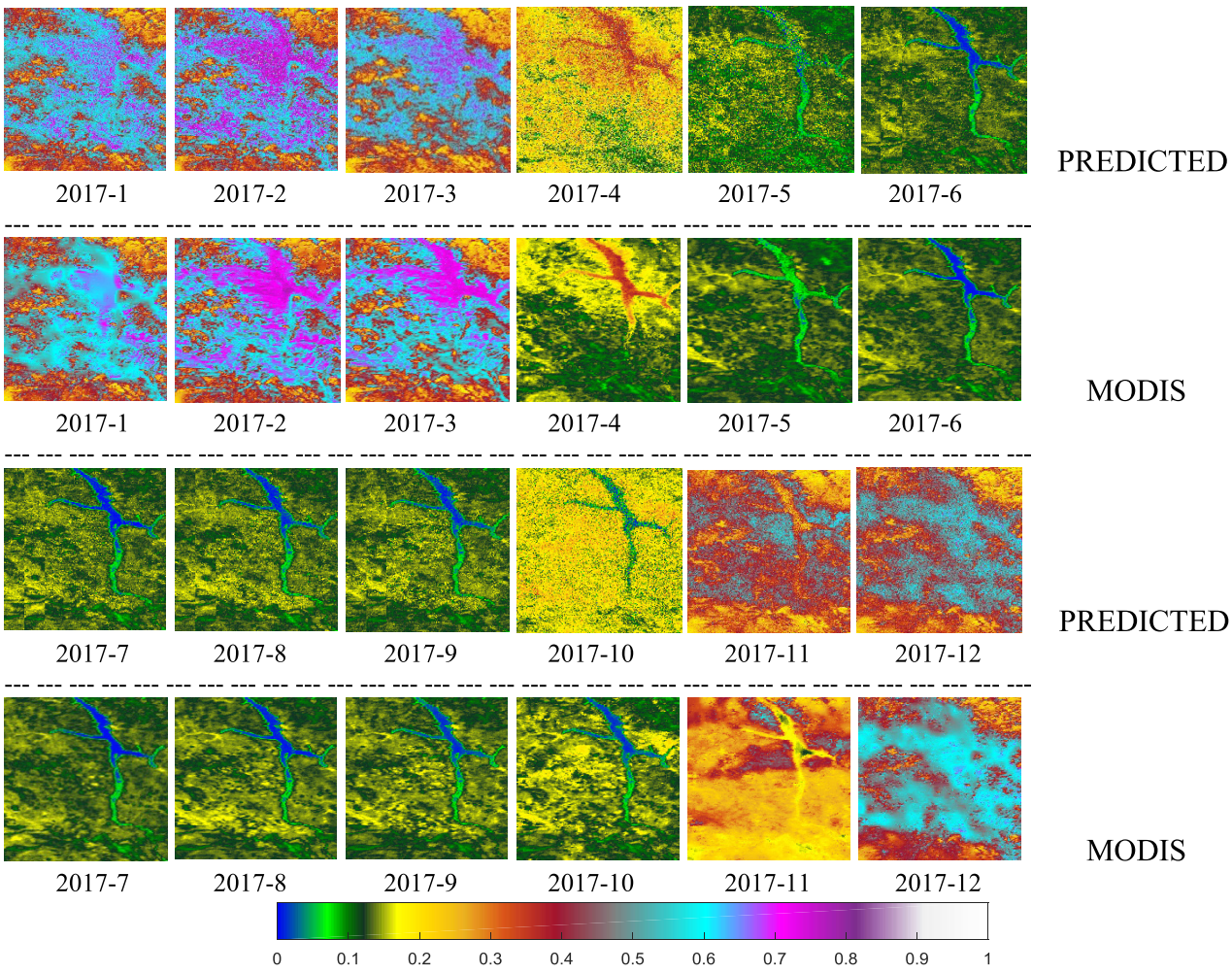

Fig. 7. Time series albedo predicted from EEMD-NARnet and the MODIS albedo in a snowy area. The month is indicated for each monthly albedo map (YEAR-MONTH).

time series varies simultaneously. Fig. 6 shows the scatterplot of monthly average albedo predicted from EEMD-NARnet and monthly MODIS albedo product. For each month, the pixel-value-based scatterplot exhibits a good agreement with the RMSE from 0.0045 to 0.0052 and the R^2 from 0.8929 to 0.9311, which indicates that the EEMD-NARnet model works well for monthly albedo prediction in snow-free areas.

C. Monthly Albedo Prediction for a Snowy Area

Snowfall is an important factor that causes a dramatic fluctuations in land surface albedo, and it hinders the prediction of time series albedo due to its irregularity. In this article, the EEMD-NARnet model is employed to forecast time series albedo over the snowy area in Under-Khuan. Fig. 7 shows the prediction results in a 200 × 200 pixel (100 × 100 km) area in 2017. In the snowy area, the albedo value is high in the nongrowing season and low during the growing period. Compared with MODIS albedo data, the predicted result can capture the albedo variation pattern both in the snowy period and the growing season. The spatial distribution pattern is also consistent with MODIS data. However, a slight overestimation exists in April, October, and November, which occurs in all land cover types.

Fig. 8 shows the scatter plot of predicted albedo and MODIS product for each month. Overall, the prediction has high accuracy, RMSE of the snow-free period (May–September) ranges from 0.0127 to 0.0249. For the snowy period, the situation is more complex: from December to the following March, the average temperature of these months is −12 °C, and the land surface has consistent snow cover, the albedo value is high. In April, October, and November, overestimation occurs. In this area, April is the local snowmelt season, October and November comprise the local snowfall season, and the average temperature is 5 °C. The emergence and melting of snow promotes a rapid surface change, which makes the prediction more difficult [51].

In the snowy area, the albedo prediction accuracy depends on the time span and intensity of snowfall, and other surface parameters play a very small role. Time span and intensity of snowfall affect the fluctuation of surface albedo directly; in fact, albedo is relatively stable in snowy areas throughout the year. Instead, in some mid-latitude regions, the snow cover period may last only a few days. The drastic change of surface albedo will bring great errors to the prediction.

Fig. 9 shows the annual variation of average April albedo over the different land surface types in Table II. From

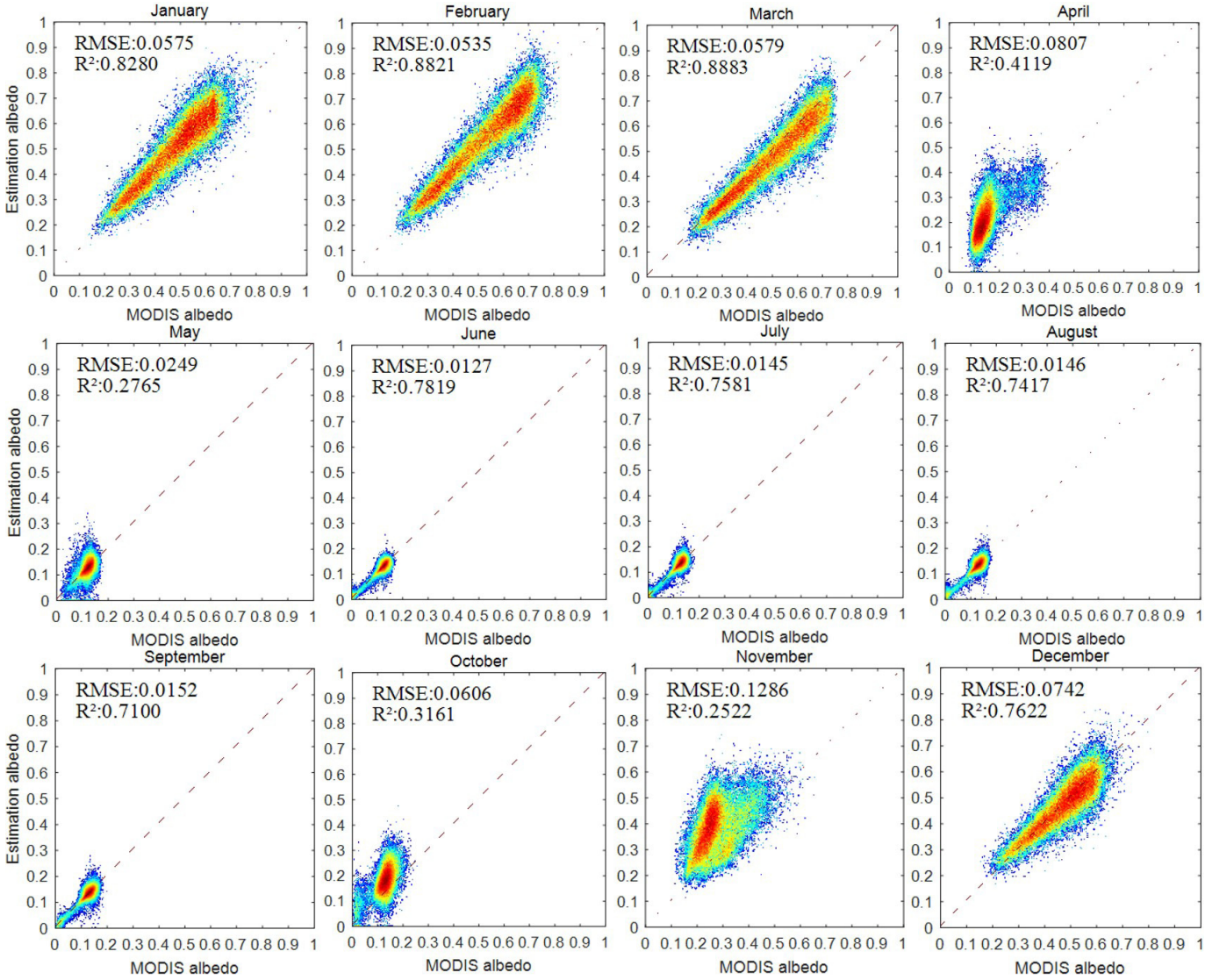

Fig. 8. Scatterplot and statistics for a snowy area; the density plot uses color from blue to red to represent density from low to high.

2001 to 2016, the increase of land surface albedo caused by snowfall is more obvious, especially in 2006 and 2010. The prediction algorithm depends on the trend of historical data, and when recent data are out of the cycle of historical change, the estimated results will produce large deviations. In April 2017, the snowfall in this area decreased significantly, so a higher estimation was produced. Overestimation in October and November can be explained accordingly.

Another important factor which causes prediction error is human activities. Fig. 10 shows the scatterplot of the estimated albedo and MODIS albedo product for different land cover pixels. From Fig. 10, we can see that the albedo is overestimated in snowy urban area, which is mainly due to unpredictable human activities in this area. The prediction accuracy is better for vegetation lands than urban lands.

D. Daily Albedo Prediction at Snow-Free and Snowy Area

Monthly albedo, derived by averaging and filling the MCD43A3 time series, exhibits a certain degree of smoothness and periodicity. The mutability of daily albedo is prominent, especially in the cropland area. MCD43D3 provides albedo products with a time resolution of one day. To verify the adaptability of the algorithm in a more complex and unstable time series, the EEMD-NARnet model is used to forecast the daily albedo time series in several different land cover types. In this experiment, pixels for monthly prediction validation were also used to validate daily predictions at both snow-free area and snowy areas. For both snow-free and snowy pixels, albedos from the same day of every year from 2001 to 2016 are combined into a new time series, and the daily albedo for the year 2017 is forecast. Based on the EEMD technology, each time series is decomposed into a set of stable and linear sequences, which concentrate the most significant and important information from the original sequence. Decomposition results from EEMD are used in the NARnet to forecast time series albedo in 2017.

Fig. 11 shows the verification of estimation results derived from the EEMD-NARnet method and MODIS daily albedo

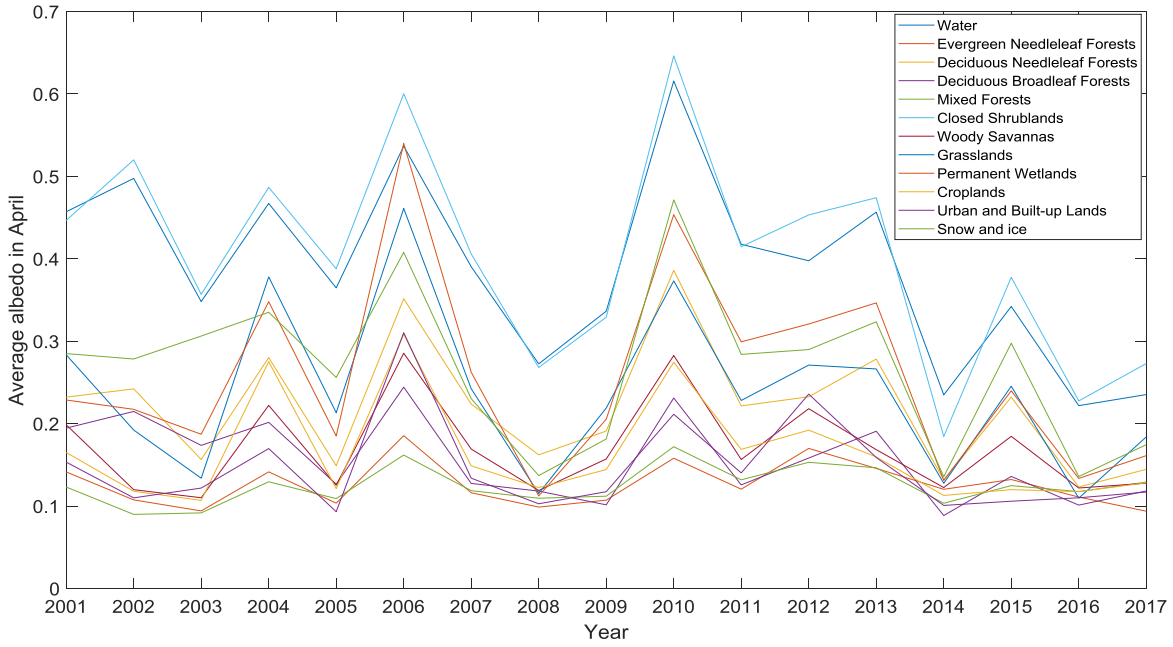

Fig. 9. Annual variation curve of average April albedo over different surface types in Table II.

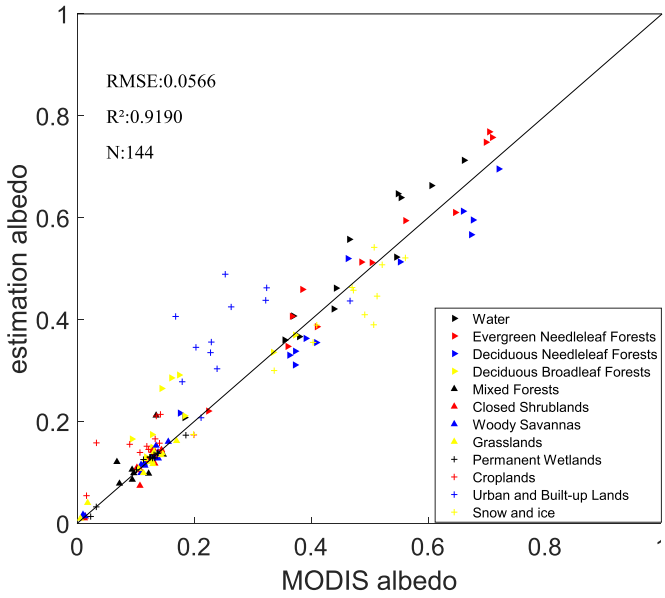

Fig. 10. Verification of estimation with the MODIS monthly albedo product on snow-covered pixels.

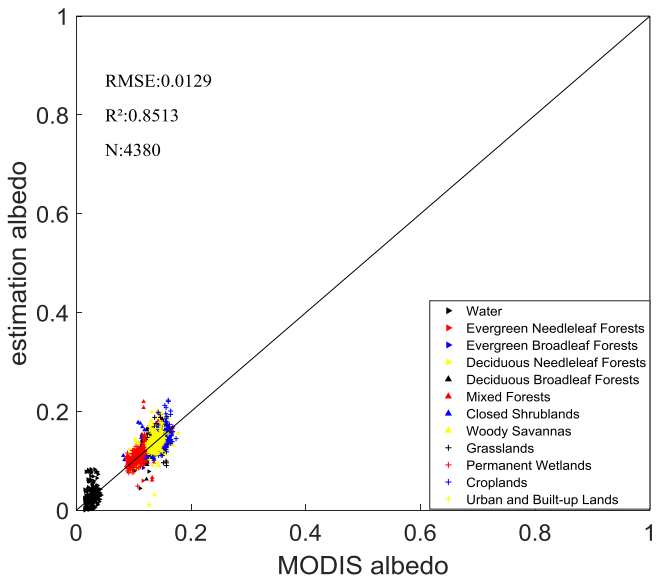

Fig. 11. Verification of estimation with MODIS daily albedo on snow-free pixels.

at a snow-free area. The time series prediction and MODIS albedo are in very good agreement during the entire year in each land cover type, with RMSE and R^2 of 0.0129 and 0.8513, respectively. The forecasting method has a better performance when applied to vegetation surfaces compared to water surfaces. Meanwhile, slightly worse predictions were found in urban areas, as it is difficult to predict the sudden change in albedo caused by human activities on a short time scale.

Fig. 12 shows that the estimation results have a good correlation with MODIS daily albedo in snowy areas, with an RMSE and R^2 of 0.0759 and 0.8651, respectively. Part of the daily albedo forecasting results exhibits overestimation and underestimation in snowy areas, especially when the albedo value is high. During the snowy period, the MODIS time series albedo shows strong mutability, and this mutation has no regular rule at the short time scale. Compared with the time series albedo in snow-free areas, the albedo series affected by snow cover shows dramatic fluctuations. This is why the albedo prediction for snowy areas presented a larger uncertainty. Even so, after reorganizing the time series, the EEMD-NARnet method can still generate reasonable time series albedo prediction values.

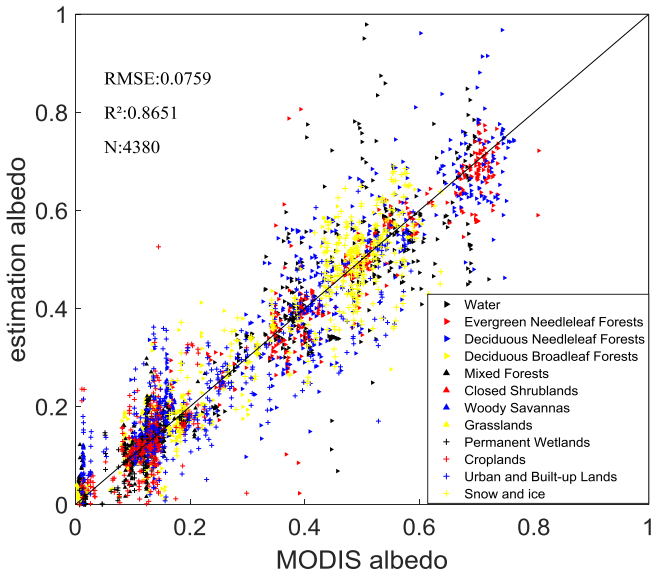

Fig. 12. Verification of estimation with MODIS daily albedo on snowy pixels.

V. Discussion

A. Error Induced by Land Surface Changes

Land surface characteristic is important for accurate forecasting as it domains the albedo variation pattern. In snow-free area, vegetation growth is the main factor affecting the land surface changes, and this change is seasonal in the absence of natural disasters. The low value of the albedo time series occurs around in the month when vegetation grows most vigorously. Seasonal variation is not obvious between years in grasslands, and it shows a slow upward trend in woodlands. Even in cropland areas, land cover type changes from crop harvesting are also regular [52], and this periodic change will not introduce large errors in albedo prediction.

In snowy areas, land cover change can be divided into three periods: snow cover; snowfall/snowmelt; and snow-free. Figs. 8 and 9 show that large prediction error occurs in the snowfall/snowmelt period (April, May, October, and November). In this special period, land surface situation (snow covered or not) differs year by year, so it is difficult to learn from the historical data and give a reasonable forecast. the EEMD-NARnet method, which depends heavily on the historical time series, cannot account for such large changes, and the application of this method is limited. To improve the prediction of this period, more information about the land surface should be introduced.

B. Applicability for High Spatio-Temporal Data

As the model is constructed on pixel scale and based only on historical time series data, it can be easily applied to forecast higher spatial and temporal resolution albedo. Though albedo data may fluctuate intensively with the increase of spatial and temporal resolution, this fluctuation can also be considered as more detailed information of the data set. Once the periodical change pattern exists, the EEMD-NARnet can exhibit a good performance.

However, when applying this method to snowy areas, with the improvement of spatial and temporal resolution, the irregular sudden change may greatly increase; in this case, it is hard to find the regularity from the historical data, and the prediction accuracy may reduce accordingly, especially in the snowmelt and snowfall periods.

C. Applicability for Other Land Surface Parameters Forecast

MCD43A3 albedo products have been produced since 2001 with a temporal resolution of one day. The long time series and high temporal resolution data set provides the possibility for us to analyze land surface change and to predict and evaluate future time series [37]. As an adaptive time–frequency localization analysis method, the EEMD technology eliminates the limitation of the Fourier transform and couples perfectly with the MODIS time series albedo. This method can be applied to other land surface parameters, such as LAI and normalized difference vegetation index (NDVI).

VI. Conclusion

This article developed an EEMD-NARnet model for decomposing historical albedo time series data to predict future values. Using the EEMD technology, albedo time series data were decomposed into several components which had a particular frequency or time scale. Different NARnet models were constructed with each subseries, and the final predicted albedos were obtained by conjunction of these models. The input to the EEMD-NARnet was the time-series MODIS albedo only, and the output was the future albedo time series. EEMD-NARnet model was constructed for both snow-free and snowy areas; monthly and daily albedo were forecast with the proposed model.

The EEMD-NARnet method is able to forecast temporally continuous albedo in snow-free areas for all land surface types. The predicted albedo and MODIS albedo have good consistency. In snowy areas, the proposed method also shows high prediction accuracy in snow-free and snowy periods, accuracy decreased due to the irregular change pattern of the land surface during the snowfall/snowmelt period. After all, the proposed model can generate accurate and stable forecasting results for most situations. For snowfall and snowmelt periods, more land surface information should be introduced, adjusting the model over time may also be an effective way to improve the performance.

Compared with traditional prediction methods, the EEMD-NARnet approach has unique advantages. First, it uses the EEMD decomposition technique to better depict the trends and periodic characteristics of the data time series, which can efficiently simplify the forecasting. Second, no exogenous data is needed for forecasting, which makes the forecasting simple and flexible. Third, it can forecast albedo time series over both snow-free and snowy surfaces with high accuracy. Finally, it can be easily extended to other land surface parameters, such as LAI, NDVI, etc.

REFERENCES

[1] S. Liang, K. Wang, X. Zhang, and M. Wild, "Review on estimation of land surface radiation and energy budgets from ground measurement, remote sensing and model simulations," *IEEE J. Sel. Topics Appl. Earth Observ. Remote Sens.*, vol. 3, no. 3, pp. 225–240, Sep. 2010.

[2] B. Pinty *et al.*, "Partitioning the solar radiant fluxes in forest canopies in the presence of snow," *J. Geophys. Res. Atmos.*, vol. 113, no. D4, 2008, Art. no. D04104.

[3] Y. Shuai *et al.*, "Approach for the long-term 30-m land surface snow-free albedo retrieval from historic Landsat surface reflectance and MODIS-based a priori anisotropy knowledge," *Remote Sens. Environ.*, vol. 152, pp. 467–479, Sep. 2014.

[4] C. Schaaf *et al.*, "Retrieval of surface albedo from satellite sensors," in *Advances in Land Remote Sensing: System Modeling Inversion and Application*. New York, NY, USA: Springer, 2008, pp. 219–243.

[5] R. A. Betts, "Offset of the potential carbon sink from boreal forestation by decreases in surface albedo," *Nature*, vol. 408, no. 6809, pp. 187–190, 2000.

[6] S. D. Peckham *et al.*, "Fire-induced changes in green-up and leaf maturity of the Canadian boreal forest," *Remote Sens. Environ.*, vol. 112, no. 9, pp. 3594–3603, 2008.

[7] D. A. Randall *et al.*, "A revised land surface parameterization (SiB2) for GCMS. Part III: The greening of the Colorado State University general circulation model," *J. Climate*, vol. 9, Apr. 1996.

[8] S. V. Ollinger *et al.*, "Canopy nitrogen, carbon assimilation, and albedo in temperate and boreal forests: Functional relations and potential climate feedbacks," *Proc. Nat. Acad. Sci. USA*, vol. 105, no. 49, pp. 19336–19341, Dec. 2008.

[9] J. T. Randerson *et al.*, "The impact of boreal forest fire on climate warming," *Science*, vol. 314, no. 5802, pp. 1130–1132, 2006.

[10] I. Csiszar and G. Gutman, "Mapping global land surface albedo from NOAA AVHRR," *J. Geophys. Res., Atmos.*, vol. 104, no. D6, pp. 6215–6228, 1999.

[11] N. C. Strugnell and W. Lucht, "An algorithm to infer continental-scale albedo from AVHRR data, land cover class, and field observations of typical BRDFs," *J. Climate*, vol. 14, no. 7, pp. 1360–1376, 2001.

[12] N. C. Strugnell, W. Lucht, and C. Schaaf, "A global albedo data set derived from AVHRR data for use in climate simulations," *Geophys. Res. Lett.*, vol. 28, no. 1, pp. 191–194, 2001.

[13] W. Lucht, C. B. Schaaf, and A. H. Strahler, "An algorithm for the retrieval of albedo from space using semiempirical BRDF models," *IEEE Trans. Geosci. Remote Sens.*, vol. 38, no. 2, pp. 977–998, Mar. 2000.

[14] S. Liang *et al.*, "A long-term Global LAnd Surface Satellite (GLASS) data-set for environmental studies," *Int. J. Digit. Earth*, vol. 6, pp. 5–33, Dec. 2013.

[15] B. Jiang *et al.*, "Analysis and prediction of MODIS LAI time series with dynamic harmonic regression model," *J. Remote Sens.*, vol. 14, no. 1, pp. 13–32, 2010.

[16] M. L. Berbet and M. H. Costa, "Climate change after tropical deforestation: Seasonal variability of surface albedo and its effects on precipitation change," *J. Climate*, vol. 16, no. 12, pp. 2099–2104, 2003.

[17] S. Boussetta *et al.*, "Assimilation of surface albedo and vegetation states from satellite observations and their impact on numerical weather prediction," *Remote Sens. Environ.*, vol. 163, pp. 111–126, Jun. 2015.

[18] B. Jiang *et al.*, "Modeling MODIS LAI time series using three statistical methods," *Remote Sens. Environ*, vol. 114, no. 7, pp. 1432–1444, 2010.

[19] S. Cristina *et al.*, "MERIS phytoplankton time series products from the SW Iberian Peninsula (Sagres) using seasonal-trend decomposition based on loess," *Remote Sens.*, vol. 8, no. 6, p. 449, 2016.

[20] H. Zhou *et al.*, "Extended data-based mechanistic method for improving leaf area index time series estimation with satellite data," *Remote Sens.*, vol. 9, no. 6, p. 533, 2017.

[21] W.-C. Wang, K.-W. Chau, D.-M. Xu, and X.-Y. Chen, "Improving forecasting accuracy of annual runoff time series using ARIMA based on EEMD decomposition," *Water Resour. Manage.*, vol. 29, no. 8, pp. 2655–2675, 2015.

[22] X. Xu *et al.*, "Assimilation of SMOS soil moisture in the MESH model with the ensemble Kalman filter," in *Proc. IEEE Int. Geosci. Remote Sens. Symp.*, Jul. 2014, pp. 3766–3769.

[23] Z. Xiao, S. Liang, J. Wang, J. Song, and X. Wu, "A temporally integrated inversion method for estimating leaf area index from MODIS data," *IEEE Trans. Geosci. Remote Sens.*, vol. 47, no. 8, pp. 2536–2545, Aug. 2009.

[24] A. V. M. Ines, N. N. Das, J. W. Hansen, and E. G. Njoku, "Assimilation of remotely sensed soil moisture and vegetation with a crop simulation model for maize yield prediction," *Remote Sens. Environ.*, vol. 138, pp. 149–164, Nov. 2013.

[25] T. Sauter, B. Weitzenkamp, and C. Schneider, "Spatio-temporal prediction of snow cover in the Black Forest mountain range using remote sensing and a recurrent neural network," *Int. J. Climatol.*, vol. 30, no. 15, pp. 2330–2341, 2010.

[26] X. Zhang *et al.*, "A comparison study on electric vehicle growth forecasting based on grey system theory and NAR neural network," in *Proc. Smart Grid Comm. Special Session, Emerg. Techn. Syst. Secur. Market Manage. Smart Grids*, Sydney, NSW, Australia, 2016, pp. 711–715.

[27] N. E. Huang and Z. Wu, "A review on Hilbert-Huang transform: Method and its applications to geophysical studies," *Rev. Geophys.*, vol. 46, no. 2, 2008, Art. no. RG2006.

[28] X. Zhang, K. K. Lai, and S.-Y. Wang, "A new approach for crude oil price analysis based on empirical mode decomposition," *Energy Econ.*, vol. 30, no. 3, pp. 905–918, May 2008.

[29] Y.-F. Sang, Z. Wang, and C. Liu, "Period identification in hydrologic time series using empirical mode decomposition and maximum entropy spectral analysis," *J. Hydrol.*, vol. 424, pp. 154–164, Mar. 2012.

[30] L. Tian, J. Wang, H. Zhou, and Z. Xiao, "MODIS NBAR time series modeling with two statistical methods and application to leaf area index recursive estimation," *IEEE J. Sel. Topics Appl. Earth Observ. Remote Sens.*, vol. 8, no. 4, pp. 1404–1412, Apr. 2015.

[31] X. Li and A. H. Strahler, "Geometric-optical bidirectional reflectance modeling of the discrete crown vegetation canopy: Effect of crown shape and mutual shadowing," *IEEE Trans. Geosci. Remote Sens.*, vol. 30, no. 2, pp. 276–292, Mar. 1992.

[32] F. Maignan, F. M. Bréon, and R. Lacaze, "Bidirectional reflectance of Earth targets: Evaluation of analytical models using a large set of spaceborne measurements with emphasis on the Hot Spot," *Remote Sens. Environ.*, vol. 90, no. 2, pp. 210–220, Mar. 2004.

[33] J.-L. Roujean, M. Leroy, and P.-Y. Deschamps, "A bidirectional reflectance model of the earth's surface for the correction of remote sensing data," *J. Geophys. Res., Atmos.*, vol. 97, no. D18, pp. 20455–20468, 1992.

[34] W. Wanner, X. Li, and A. Strahler, "On the derivation of kernels for kernel-driven models of bidirectional reflectance," *J. Geophys. Res. Atmos.*, vol. 100, no. D10, pp. 21077–21089, 1995.

[35] C. B. Schaaf *et al.*, "First operational BRDF, albedo nadir reflectance products from MODIS," *Remote Sens. Environ.*, vol. 83, nos. 1–2, pp. 135–148, 2002.

[36] J. G. Salomon, C. B. Schaaf, A. H. Strahler, F. Gao, and Y. Jin, "Validation of the MODIS bidirectional reflectance distribution function and albedo retrievals using combined observations from the Aqua and Terra platforms," *IEEE Trans. Geosci. Remote Sens.*, vol. 44, no. 6, pp. 1555–1565, Jun. 2006.

[37] N. Svacina, C. Duguay, and J. King, "Modelled and satellite-derived surface albedo of lake ice—Part II: Evaluation of MODIS albedo products," *Hydrol. Processes.*, vol. 28, no. 16, pp. 4562–4572, 2014.

[38] Z. Wang *et al.*, "Using MODIS BRDF and albedo data to evaluate global model land surface albedo," *J. Hydrometeorol.*, vol. 5, no. 1, pp. 3–14, 2004.

[39] P. Lewis and M. Barnsley, "Influence of the sky radiance distribution on various formulations of the earth surface albedo," in *Proc. Conf. Phys. Measures Signals*, 1994, pp. 707–715.

[40] S. Liang, A. H. Strahler, and C. Walthall, "Retrieval of land surface albedo from satellite observations: A simulation study," *J. Appl. Meteorol.*, vol. 38, no. 6, pp. 712–725, 1999.

[41] J. Stroeve *et al.*, "Accuracy assessment of the MODIS 16-day albedo product for snow: Comparisons with Greenland *in situ* measurements," *Remote Sens. Environ.*, vol. 94, no. 1, pp. 46–60, 2005.

[42] C. B. Schaaf, J. Liu, F. Gao, and A. H. Strahler, "MODIS albedo and reflectance anisotropy products from Aqua and Terra," in *Land Remote Sensing and Global Environmental Change: NASA's Earth Observing System and the Science of ASTER and MODIS, Remote Sensing and Digital Image Processing Series*, B. Ramachandran, C. O. Justice, and M. J. Abrams, Eds. New York, NY, USA: Springer-Verlag, 2011, pp. 549–561.

[43] G. Zhang *et al.*, "Time series high-resolution land surface albedo estimation based on the ensemble Kalman filter algorithm," *Remote Sens.*, vol. 11, no. 7, p. 753, 2019.

[44] Y. Shi *et al.*, "A prior knowledge-based method to derive high-resolution leaf area index maps with limited field measurements," *Remote Sens.*, vol. 9, no. 1, p. 13, 2016.

[45] P. J. J. Luukko, J. Helske, and E. Räsänen, "Introducing libeemd: A program package for performing the ensemble empirical mode decomposition," *Comput. Stat.*, vol. 31, no. 2, pp. 545–557, 2016.
[46] N. E. Huang, Z. Shen, and S. R. Long, "A new view of nonlinear water waves: The Hilbert spectrum," *Annu. Rev. Fluid Mech.*, vol. 31, pp. 417–457, Jan. 1999.
[47] Y. Lei, Z. He, and Y. Zi, "Application of the EEMD method to rotor fault diagnosis of rotating machinery," *Mech. Syst. Signal Process.*, vol. 23, no. 4, pp. 1327–1338, 2009.
[48] Z. Wu and N. E. Huang, "Ensemble empirical mode decomposition: A noise-assisted data analysis method," *Adv. Adapt. Data Anal.*, vol. 1, no. 1, pp. 1–41, 2009.
[49] A. Lapedes and R. Farber, "Nonlinear signal processing using neural networks: Prediction and system modelling," in *Proc. IEEE Int. Conf. Neural Netw.*, San Diego, CA, USA, Tech. Rep. LA-UR-87-2662; CONF-8706130-4, Jun. 1987.
[50] E. L. Hestir *et al.*, "Identification of invasive vegetation using hyperspectral remote sensing in the california delta ecosystem," *Remote Sens. Environ.*, vol. 112, pp. 4034–4047, Nov. 2008.
[51] H. E. Henneman and H. G. Stefan, "Albedo models for snow and ice on a freshwater lake," *Cold Reg. Sci. Technol.*, vol. 29, no. 1, pp. 31–48, 1999.
[52] A. Wood, G. Ackland, and T. Lenton, "Mutation of albedo and growth response produces oscillations in a spatial Daisyworld," *J. Theor. Biol.*, vol. 242, no. 1, pp. 188–198, 2006.

Guodong Zhang received the B.S. degree from Henan Polytechnic University, Jiaozuo, China, in 2017, where he is currently pursuing the M.S. degree.

He is currently a Visiting Scholar with Beijing Normal University, Beijing, China. His research interests include data assimilation and inversion, and prediction of land parameters from remotely sensed data.

Hongmin Zhou (Member, IEEE) received the Ph.D. degree in remote sensing and geographic information systems from Beijing Normal University, Beijing, China, in 2018.

She is currently a Senior Engineer with the State Key Laboratory of Remote Sensing Science, Faculty of Geographical Sciences, Beijing Normal University/Chinese Academy of Sciences, Beijing. Her research interests include land surface radiation budget, land surface parameters retrieval from various remotely sensed data, and land surface products validation.

Changjing Wang received the B.S. degree from Henan Polytechnic University, Jiaozuo, China, in 2017, where he is currently pursuing the M.S. degree.

He is currently a Visiting Scholar with Beijing Normal University, Beijing, China. His research interest includes inversion and change analysis of land parameters from remotely sensed data.

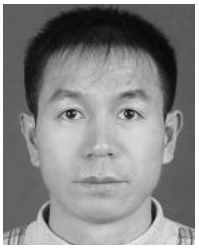

Huazhu Xue received the Ph.D. degree in cartography and geographic information systems in the area of quantitative remote sensing from the School of Geography, Beijing Normal University, Beijing, China, in 2012.

Since 2012, he has been an Assistant Professor with the School of Surveying and Land Information Engineering, Henan Polytechnic University, Jiaozuo, China. His research interests include vegetation parameters inversion, satellite image processing, and GIS applications.

Jindi Wang received the B.S. degree from the Beijing University of Posts and Telecommunications, Beijing, China, in 1982.

She is currently a Professor with the State Key Laboratory of Remote Sensing Science, Research Center for Remote Sensing and Geographic Information Systems, Beijing Normal University, Beijing. Her primary research interests focus on land surface bidirectional reflectance distribution function modeling, land surface parameter retrieval, and typical land surface objects' spectrum library building and its application.

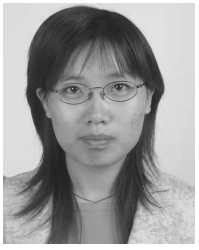

Huawei Wan received the Ph.D. degree from Beijing Normal University, Beijing, China, in 2007.

She is currently a Research Scientist with the Center for Satellite Application on Ecology and Environment, Ministry of Ecology and Environment, Beijing. Her research interests include quantitative parameters reversion, and ecosystem and biodiversity assessment based on remote sensing.